

# Linear Magnetoresistance of 2D Massless Dirac Fermions in the Quantum Limit

Xiao-Bin Qiang,<sup>1,2,\*</sup> Han-Yi Xu,<sup>1,\*</sup> Ren-Jie Tong,<sup>1,\*</sup> Shuai Li,<sup>3</sup> Zi-Xuan Gao,<sup>1</sup> Peng-Lu Zhao,<sup>4,†</sup> and Hai-Zhou Lu<sup>1,4,‡</sup>

<sup>1</sup>*State Key Laboratory of Quantum Functional Materials, Department of Physics, and Guangdong Basic Research Center of Excellence for Quantum Science, Southern University of Science and Technology (SUSTech), Shenzhen 518055, China*

<sup>2</sup>*Division of Physics and Applied Physics, School of Physical and Mathematical Sciences, Nanyang Technological University, 21 Nanyang Link, 637371, Singapore*

<sup>3</sup>*Hubei Engineering Research Center of Weak Magnetic-field Detection, Department of Physics, China Three Gorges University, Yichang 443002, China*

<sup>4</sup>*Quantum Science Center of Guangdong-Hong Kong-Macao Greater Bay Area (Guangdong), Shenzhen 518045, China*  
(Dated: December 16, 2025)

Linear magnetoresistance is a hallmark of 3D Weyl metals in the quantum limit. Recently, a pronounced linear magnetoresistance has also been observed in 2D graphene [Xin *et al.*, *Nature* **616**, 270 (2023)]. However, a comprehensive theoretical understanding remains elusive. By employing the self-consistent Born approximation, we derive the analytical expressions for the magnetoresistivity of 2D massless Dirac fermions in the quantum limit. Notably, our result recovers the minimum conductivity in the clean limit and reveals a linear dependence of resistivity on the magnetic field for Gaussian impurity potentials, in quantitative agreement with experiments. These findings shed light on the magnetoresistance behavior of 2D Dirac fermions under ultra-high magnetic fields.

## I. INTRODUCTION

Magnetoresistance refers to the variation in resistance of materials in response to an applied magnetic field. In most conventional materials, the magnetoresistance typically follows a positive quadratic dependence on the magnetic field [1]. Deviations from this standard behaviour can reveal exotic properties of materials, and provides a powerful tool for exploring underlying phenomena.

In a weak magnetic field, negative (positive) magnetoresistance is a hallmark of weak localization (antilocalization) [2–9]. In a moderate magnetic field, negative magnetoresistance can arise from the chiral anomaly [10–13] or Berry curvature [14–18]. In a higher magnetic field, Shubnikov–de Haas oscillation of magnetoresistance serves as a critical evidence for the quantum Hall effect [19–22]. Besides, in an ultra-high magnetic field, where only the zeroth Landau level is occupied (quantum limit), linear magnetoresistance emerges as a hallmark of 3D Weyl metals [23–28]. Notably, recent experiment [29] has reported a pronounced linear magnetoresistance in graphene under the quantum limit condition. Due to 2D electronic structure of graphene, where the energy spectrum is quantized into a series of Landau levels in a strong magnetic field, existing theoretical framework based on the first-order Born approximation [23, 30] fails to model this 2D system. This highlights a theoretical gap that warrants further investigation.

In this work, we present a comprehensive study of the magnetoresistance of 2D massless Dirac fermions in

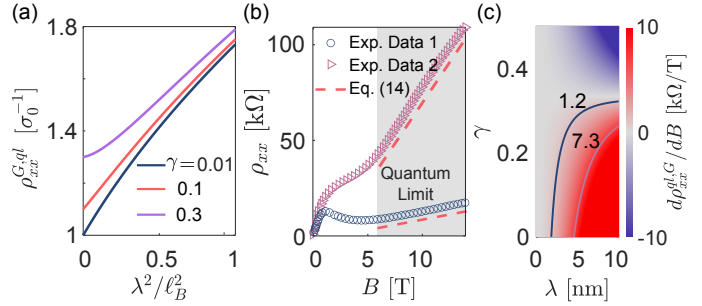


FIG. 1. (a) Calculated magnetoresistivity [Eq. (13)] as a function of the dimensionless parameter  $\lambda^2/\ell_B^2$  for various impurity strengths  $\gamma$ , where  $\lambda$  is the decay length of the Gaussian potential,  $\ell_B = \sqrt{\hbar/(eB)}$  is the magnetic length, and  $\sigma_0 = e^2/(2\sqrt{2\pi}\hbar)$  is the minimal conductivity of 2D massless Dirac fermions [31–34]. (b) Comparison between linear magnetoresistivity in the quantum limit [Eq. (14)] and experimental data [29]. (c) Phase diagram for the slope of the magnetoresistivity  $d\rho_{xx}^{G,ql}/dB$  as a function of the decay length  $\lambda$  and impurity strength  $\gamma$ . Here,  $\gamma$  cannot be zero unless  $\lambda$  approaches zero first. Two inset solid curves indicate the ranges of parameters consistent with the experimental slopes (1.2 and 7.3  $\text{k}\Omega/\text{T}$ ) shown in panel (b).

the quantum limit. Starting from linear-response theory [35] and treating impurity scattering within the self-consistent Born approximation [36–38], we derive analytical expressions for the longitudinal resistivity  $\rho_{xx}(B)$ . Our analysis includes three distinct types of impurity potentials including  $\delta$ -function potential, Gaussian potential, and Yukawa potential, each resulting in a different dependence of resistivity on the magnetic field. When the impurity strength approaches to zero, the derived results consistently converge to the well-established minimum conductivity of 2D massless Dirac fermions [31–34].

\* These authors contributed equally to this work.

† Corresponding author: zhaoplus@gmail.com

‡ Corresponding author: luhz@sustech.edu.cn

Notably, we find that the Gaussian impurity potential can exhibit a linear magnetoresistivity whenever its decay length is smaller than the magnetic length. As shown in Fig. 1, our analytical results [Eqs. (13) and (14)] are quantitatively in agreement with experimental observations [29].

## II. MODEL AND LANDAU LEVELS

The Hamiltonian of 2D massless Dirac fermions is [20, 39]

$$\mathcal{H}_0 = v\mathbf{k} \cdot \boldsymbol{\sigma}, \quad (1)$$

where  $v$  is the model parameter characterizing the Fermi velocity,  $\mathbf{k} = (k_x, k_y)$  is the wave vector, and  $\boldsymbol{\sigma} = (\sigma_x, \sigma_y)$  is the vector of Pauli matrices. This Hamiltonian serves as an effective model for a range of novel quantum materials, such as the surface states of topological insulators [40, 41] and graphene [42, 43]. In the case of graphene, it represents the effective low-energy Hamiltonian near one of the two inequivalent valleys. The counterpart valley possesses an identical Landau-level spectrum and yields equivalent physical responses in the present context. Therefore, considering a single valley is sufficient for describing the magnetotransport phenomena discussed in this work. The energy spectrum of this model [Eq. (1)] is given by  $\varepsilon_{\pm} = \pm v k$ , where  $k = |\mathbf{k}|$ . As shown in Fig. 2(a), this linear energy spectrum is a defining characteristic of 2D massless Dirac fermions and underlies a variety of novel physical properties [43–47].

In a perpendicular magnetic field  $\mathbf{B} = B\hat{z}$ , the wave vector in the Landau gauge is modified to  $\mathbf{k} = (k_x + eA_x/\hbar, i\partial_y)$  with vector potential  $\mathbf{A} = -yB\hat{x}$ , where  $-e$  is the electron charge, and  $\hbar = h/(2\pi)$  is the reduced Planck constant. Then, by introducing the ladder operators [48, 49]  $a = -[(y - y_0)/\ell_B + \ell_B\partial_y]/\sqrt{2}$  and  $a^\dagger = -[(y - y_0)/\ell_B - \ell_B\partial_y]/\sqrt{2}$  with guiding center  $y_0 = \ell_B^2 k_x$  and magnetic length  $\ell_B = \sqrt{\hbar/(eB)}$ , the Hamiltonian [Eq. (1)] becomes

$$\mathcal{H}_0 = \begin{bmatrix} 0 & (\sqrt{2}v/\ell_B)a \\ (\sqrt{2}v/\ell_B)a^\dagger & 0 \end{bmatrix}. \quad (2)$$

With trial wave functions of the form  $[0, |0\rangle]^T$  for  $n = 0$ , and  $[c_1|n-1\rangle, c_2|n\rangle]^T$  for  $n \neq 0$ , the eigenenergies are solved as (details can be found in Sec. SI of Supplemental Material [50])

$$\varepsilon_n = \pm \frac{1}{\ell_B} \sqrt{2v^2 n}, \quad n = 0, 1, 2, \dots. \quad (3)$$

As shown in Figs. 2(b) and (c), Eq. (3) represents a series of Landau levels for 2D massless Dirac fermions. Additionally, the wave functions are given by

$$\begin{aligned} \psi_{k_x, \pm n}(\mathbf{r}) &= \frac{e^{ik_x x}}{\sqrt{2L_x}} \begin{bmatrix} \phi_{k_x, n-1}(y) \\ \pm \phi_{k_x, n}(y) \end{bmatrix}, \quad n = 1, 2, \dots, \\ \psi_{k_x, 0}(\mathbf{r}) &= \frac{e^{ik_x x}}{\sqrt{L_x}} \begin{bmatrix} 0 \\ \phi_{k_x, 0}(y) \end{bmatrix}, \quad n = 0, \end{aligned} \quad (4)$$

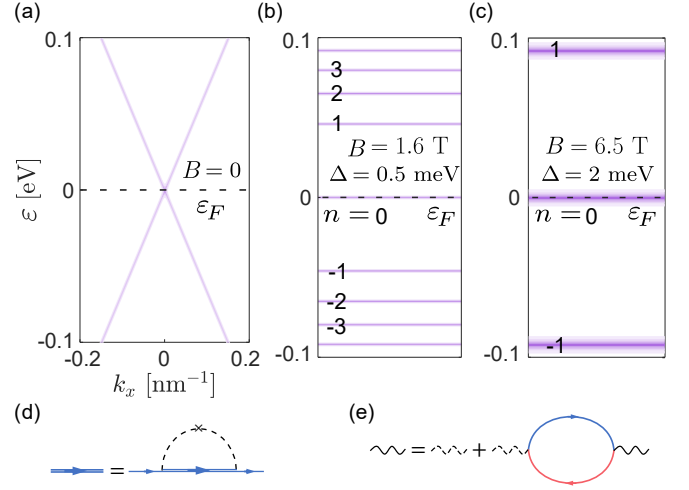


FIG. 2. Energy spectrum of massless Dirac fermions [Eq. (1)]. (a) In absence of magnetic field, (b) Landau levels with magnetic field  $B = 1.6$  T (assuming a constant line-width  $\Delta = 0.5$  meV), and (c) Landau levels with  $B = 6.5$  T and  $\Delta = 2$  meV. The Landau levels are denoted by indices  $n = 0, \pm 1, \pm 2, \dots$ . The dashed line represents the Fermi level  $\varepsilon_F$ . The model parameter is  $v = 0.65$  eV·nm adopted from Ref. [20]. Feynman diagrams for (d) the self-consistent Born approximation, and (e) the screened length  $\kappa$  of the Yukawa potential. In these diagrams, the double solid line represents the dressed Green function, while the single solid line represents the bare Green function, and the dashed line indicates impurity scattering. The solid wavy line represents interaction within the random phase approximation, and the dashed wavy line represents to the bare Coulomb interaction.

where  $L_x$  is the system length,  $\phi_{k_x, n}(y) = e^{-\zeta^2/2} H_n(\zeta)/\sqrt{n! 2^n \sqrt{\pi} \ell_B}$  with  $\zeta = (y - y_0)/\ell_B$ , and  $H_n(\zeta)$  is the Hermite polynomial.

In the quantum limit, where only the zeroth Landau level ( $\varepsilon_0 = 0$ ) is occupied, which implies that the Fermi energy is  $\varepsilon_F = 0$ . This indicates that the quantum limit coincides with the charge neutrality point. This behaviour is fundamentally different from that of a conventional 2D electron gas [51], where the lowest Landau level lies at a finite energy  $\hbar\omega/2$ , with  $\omega$  denoting the cyclotron frequency.

## III. MAGNETORESISTIVITY IN THE QUANTUM LIMIT

Following the standard linear-response theory [35], the longitudinal conductivity in the quantum limit is given by (see Sec. SII of [50])

$$\sigma_{xx}^{ql} = \frac{e^2 v^2}{8\pi\hbar\mathcal{V}} \sum_{k_x, n=\pm 1} \mathcal{A}_{k_x, 0}(\varepsilon_F) \mathcal{A}_{k_x, n}(\varepsilon_F), \quad (5)$$

where the superscript of  $\sigma_{xx}^{ql}$  denotes the quantum limit, and  $\mathcal{V}$  is the system volume. The spectral function is

given by  $\mathcal{A}_{k_x,n} = 2\Delta_{k_x,n}/[(\varepsilon_F - \varepsilon_n)^2 + \Delta_{k_x,n}^2]$ , where  $\Delta_{k_x,n}$  is the line-width function. Figs. 2(b) and (c) illustrate the impurity-dressed Landau levels [Eq. (3)] with help of the spectral function. The effect of impurity scattering is to broaden the Landau levels into finite widths.

The line-width function is generally written as  $\Delta_{k_x,n} = -\text{Im}[\Sigma_{k_x,n}^r]$ , where  $\Sigma_{k_x,n}^r$  is the impurity scattering induced selfenergy. Under the self-consistent Born approximation [36–38],  $\Sigma_{k_x,n}^r$  can be calculated from the Feynman diagram in Fig. 2(d) and is found as

$$\Sigma_{k_x,n}^r = \sum_{k'_x,n'} \frac{|\langle k'_x, n' | V(\mathbf{r}) | k_x, n \rangle|^2}{\varepsilon_F - \varepsilon_{n'} - \Sigma_{n'}^r}. \quad (6)$$

Here, the scattering matrix element is given by

$$\langle k'_x, n' | V(\mathbf{r}) | k_x, n \rangle = \int d\mathbf{r} \psi_{k'_x, n'}^\dagger(\mathbf{r}) V(\mathbf{r}) \psi_{k_x, n}(\mathbf{r}), \quad (7)$$

where  $\psi_{k_x, n}(\mathbf{r})$  is the wave function of Landau level given by Eq. (4),  $V(\mathbf{r}) = \sum_i U(\mathbf{r} - \mathbf{r}_i)$  is the total impurity potential, and  $U(\mathbf{r} - \mathbf{r}_i)$  is the potential due to a single impurity randomly located at position  $\mathbf{r}_i$ . The explicit form of  $U(\mathbf{r} - \mathbf{r}_i)$  depends on the specific type of impurity potential considered. For simplicity, we assume that different types of impurity are uncorrelated, and their contributions to the total resistivity are additive [52].

After solving the self-consistent equation, performing the ensemble average [53], and converting the summation over  $k_x$  to the Landau level degeneracy via  $(1/\mathcal{V}) \sum_{k_x} \rightarrow 1/(2\pi\ell_B^2)$  (see Sec. SII of [50]), the conductivity [Eq. (5)] is simplified to

$$\sigma_{xx}^{ql} = \frac{e^2}{4\pi\hbar} \sum_{n=\pm 1} \sqrt{\frac{\vartheta_n}{\vartheta_0}} \frac{1}{1 + \vartheta_n/\varepsilon_n^2}, \quad (8)$$

where  $\varepsilon_n$  is given by Eq. (3). All aspects concerning impurity scattering are incorporated in the function  $\vartheta_n$  ( $n \in \{0, \pm 1\}$ ), which is defined by

$$\vartheta_n = \frac{n_i}{4|n|} \int \frac{d\mathbf{q}}{(2\pi)^2} u_{\mathbf{q}} u_{-\mathbf{q}} e^{-q^2 \ell_B^2/2} (\ell_B q)^{2|n|}, \quad (9)$$

where  $n_i$  is the impurity density, and  $u_{\mathbf{q}}$  is the Fourier transform of the impurity potential, i.e.,  $u_{\mathbf{q}} = \int d\mathbf{r} e^{-i\mathbf{q} \cdot \mathbf{r}} U(\mathbf{r})$ .

This expression [Eq. (8)] can be applicable to all types of impurity potentials, and is the central result of our work. In the quantum limit, the Fermi level only cuts the zeroth Landau level, which corresponds to a charge neutral point for 2D massless Dirac fermions. At this point, the Hall conductivity vanishes, and the magnetoresistivity simply reduces to  $\rho_{xx}^{ql} = 1/\sigma_{xx}^{ql}$ .

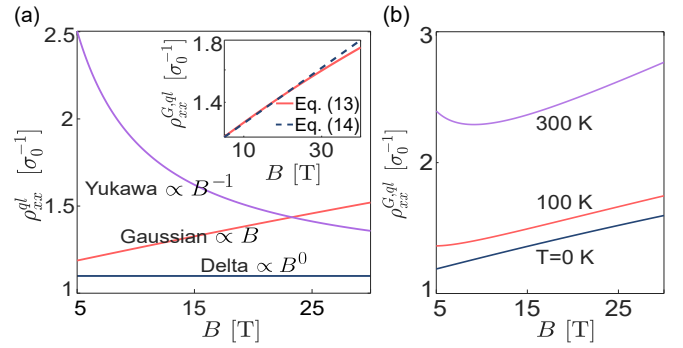


FIG. 3. (a) Comparison of calculated magnetoresistivities for different impurity potentials, as given by Eqs. (11), (13), and (16). The impurity strength is set to  $\gamma = 0.1$  for both the  $\delta$ -function and Gaussian potentials. The decay length is taken  $\lambda = 4$  nm for the Gaussian potential. For the Yukawa potential, the impurity density is taken  $n_i = 0.1 \text{ nm}^{-2}$ . The other parameters are  $\mathcal{C} \simeq 0.2$  and  $g \simeq 1.22$  by adopting the experimental values  $v = 0.65 \text{ eV}\cdot\text{nm}$  [20] and  $\epsilon = 6.9\epsilon_0$  [54]. The inset compares the original magnetoresistivity [Eq. (13)] with the approximated expression [Eq. (14)] for the Gaussian potential. (b) Finite-temperature magnetoresistivity for the Gaussian potential at  $T = 0 \text{ K}$ ,  $100 \text{ K}$ , and  $300 \text{ K}$ .

#### IV. MAGNETORESISTIVITY FOR DIFFERENT IMPURITY POTENTIALS

##### A. $\delta$ -function potential

For the simplest case, we first consider the point-like  $\delta$ -function potential (also known as the white noise). It takes the form

$$U(\mathbf{r} - \mathbf{r}_i) = u_0 \delta(\mathbf{r} - \mathbf{r}_i) \quad (10)$$

with a constant  $u_0$ , and the corresponding Fourier component is  $u_{\mathbf{q}} = u_0$ . By substituting  $u_{\mathbf{q}}$  into Eq. (9), we first obtain  $\vartheta_0 = n_i u_0^2 / (2\pi\ell_B^2)$  and  $\vartheta_{\pm 1} = n_i u_0^2 / (4\pi\ell_B^2)$ . Then, inserting  $\vartheta_0$  and  $\vartheta_{\pm 1}$  into Eq. (8) and taking inverse of  $\sigma_{xx}^{ql}$ , the resistivity is given by

$$\rho_{xx}^{ql,\delta} = \sigma_0^{-1} (1 + \gamma), \quad (11)$$

where  $\sigma_0 = e^2 / (2\sqrt{2}\pi\hbar)$  is the well-known minimal conductivity for 2D massless Dirac fermions [31–34], and  $\gamma = n_i u_0^2 / (8\pi v^2)$  is a dimensionless quantity characterizing the impurity strength. Notably, this result is independent of the magnetic field. In the clean limit,  $\gamma \rightarrow 0$ , the resistivity  $\rho_{xx}^{ql,\delta}$  simply reduces to  $\sigma_0^{-1}$ .

##### B. Gaussian potential

In contrast to the  $\delta$ -function potential, the Gaussian potential has a finite spatial spread and represents a long-range impurity. A typical form is given by

$$U(\mathbf{r} - \mathbf{r}_i) = u_0 \left( \frac{1}{\sqrt{2\pi\lambda}} \right)^2 e^{-\frac{|\mathbf{r} - \mathbf{r}_i|^2}{2\lambda^2}}, \quad (12)$$

where  $\lambda$  is the decay length. Its corresponding Fourier component is given by  $u_{\mathbf{q}} = u_0 e^{-q^2 \lambda^2/2}$ . Accordingly, by using Eq. (8), the longitudinal resistivity reads

$$\rho_{xx}^{ql,G} = \sigma_0^{-1} \sqrt{1 + 2\lambda^2/\ell_B^2} \left[ 1 + \frac{\gamma}{(1 + 2\lambda^2/\ell_B^2)^2} \right], \quad (13)$$

where the impurity strength  $\gamma$  shares same definition with  $\delta$ -function impurity. Fig. 1(a) shows the behaviour of  $\rho_{xx}^{ql,G}$  as a function of the dimensionless parameter  $\lambda^2/\ell_B^2$  for different values of  $\gamma$ .

In the limit  $\lambda \rightarrow 0$ , the expression reduces to the result for the  $\delta$ -function potential [Eq. (11)]. When the decay length  $\lambda$  is smaller than the magnetic length  $\ell_B$ , the resistivity  $\rho_{xx}^{ql,G}$  [Eq. (13)] can be approximately expanded as

$$\rho_{xx}^{ql,G} \simeq \sigma_0^{-1} \left[ 1 + \gamma + (1 - 3\gamma) \frac{\lambda^2 e B}{\hbar} \right], \quad (14)$$

where the magnetic length, defined as  $\ell_B = \sqrt{\hbar/eB}$ , has been substituted into the expression. As shown in the inset of Fig. 3(a), this expression [Eq. (14)] exhibits excellent agreement with Eq. (13) across a broad range of magnetic fields. Notably, Eq. (14) predicts a linear magnetoresistivity dependence on the magnetic field, with a slope given by  $d\rho_{xx}^{ql,G}/dB = 4\sqrt{2\pi^2\lambda^2(1-3\gamma)}/e$ . Importantly, this linear magnetoresistance is a characteristic feature of 2D massless Dirac fermions with linear dispersion and does not occur in conventional 2D electron gases with quadratic dispersion (see Sec. SIII of [50]).

To validate our theoretical framework, we analyze two representative experimental datasets from Ref. [29], which has reported characteristic slopes of 1.2 and 7.3  $\text{k}\Omega/\text{T}$  in the magnetoresistance measurements. As demonstrated in Fig. 1(b), our analytical result for  $\rho_{xx}^{ql,G}$  [Eq. (14)] successfully reproduces both the observed linear magnetoresistance behavior and, more importantly, quantitatively matches these distinct slopes. Additionally, as shown in the phase diagram of Fig. 1(c), our results accommodate a wide range of parameters that yield agreement with the experimental observations.

### C. Yukawa potential

Finally, we consider the Yukawa potential (also known as the screened Coulomb potential), which describes the interaction between charge carriers and ionized impurities due to the screening effect in solids [23]. This potential takes the form

$$U(\mathbf{r} - \mathbf{r}_i) = \frac{e^2}{4\pi\epsilon|\mathbf{r} - \mathbf{r}_i|} e^{-\kappa|\mathbf{r} - \mathbf{r}_i|}, \quad (15)$$

where  $\epsilon$  is the effective permittivity, and  $\kappa$  is the inverse screening length (i.e., the Thomas–Fermi wavevector) [1, 53]. Within the random phase approximation [Fig. 2(e)] [23, 35, 55], the inverse screening length is given by  $\kappa = e^2/(2\pi\epsilon\ell_B v)$  (see Sec. SII of [50]).

The corresponding Fourier component takes the form  $u_{\mathbf{q}} = e^2/(2\epsilon\sqrt{q^2 + \kappa^2})$ . Substituting  $u_{\mathbf{q}}$  into Eq. (8), the magnetoresistivity is obtained as

$$\rho_{xx}^{ql,Y} = \frac{\sigma_0^{-1}}{\sqrt{1/(ge^C) + C}} \left[ 1 + \frac{\pi n_i \ell_B^2}{8} C(1 + ge^C C) \right], \quad (16)$$

where  $g$  denotes the incomplete gamma function evaluated at the dimensionless parameter  $C$ , where  $C = e^4/(8\pi^2\epsilon^2 v^2)$  is a  $B$ -independent dimensionless constant.

In the limiting case  $C \rightarrow 0$ , the expression again reduces to the result for the  $\delta$ -function potential. Since  $\ell_B^2 = \hbar/(eB)$ , the magnetoresistivity for the Yukawa potential follows  $\rho_{xx}^{ql,Y} \propto B^{-1}$  as shown in Fig. 3(a). This behaviour contrasts sharply with the case of 3D Weyl metals, where the Yukawa potential gives rise to a linear magnetoresistivity [23].

## V. DISCUSSION AND CONCLUSION

Magnetoresistance constitutes a foundational tool for exploring the emergent properties of quantum materials. However, a consistent and detailed microscopic understanding of this phenomenon remains elusive across various platforms. 2D Dirac fermions in the quantum limit provide an analytically accessible platform for such investigations. Based on a concrete microscopic derivation, we obtain analytical expressions [Eqs. (11), (13), and (16)] for magnetoresistivity arising from different impurity potentials. As shown in Fig. 3(a), these potentials yield qualitatively different magnetic-field dependencies. Although the material-specific parameters dictate the detailed characteristics, the functional dependence on the magnetic field itself is universal.

All the above results are obtained at zero temperature. Taking the Gaussian potential as a representative case, we evaluate the magnetoresistivity at finite temperatures by incorporating the Fermi–Dirac distribution,  $\rho_{xx}^{ql,G}(T, B) = \int d\varepsilon \rho_{xx}^{ql,G}(0, B) [-\partial f_0/(\partial\varepsilon)]$ , where  $\rho_{xx}^{ql,G}(0, B)$  is the magnetoresistivity at zero temperature [Eq. (13)],  $f_0$  is the Fermi–Dirac distribution. As shown in Fig. 3(b), even at the room temperature (300 K), the magnetoresistivity exhibits a robust linear dependence on the magnetic field over a wide range.

In conclusion, by combining the linear-response theory with the self-consistent Born approximation, we obtain the analytical expressions for the longitudinal magnetoresistivity of 2D massless Dirac fermions in the quantum limit. We show that the  $\delta$ -function potential yields a field-independent resistivity, which successfully recovers the minimal conductivity of 2D massless Dirac fermions. The Gaussian potential produces a pronounced linear magnetoresistivity, which quantitatively matches the experimental observations. Finally, the Yukawa potential gives rise to a  $B^{-1}$ -dependence, which is totally distinct from the known behaviour in the 3D system. These results bridge the theoretical gap of magnetoresistance for 2D massless Dirac fermions in the quantum limit.

## ACKNOWLEDGMENTS

This work is supported by the National Key R&D Program of China (2022YFA1403700), the National Natural Science Foundation of China (12304074, 12350402, and 12525401), Guangdong Basic and Applied Basic Research Foundation (2023B0303000011), Guang-

dong Provincial Quantum Science Strategic Initiative (GDZX2201001 and GDZX2401001), the Science, Technology and Innovation Commission of Shenzhen Municipality (ZDSYS20190902092905285), High-level Special Funds (G03050K004), the New Cornerstone Science Foundation through the XPLORER PRIZE, and Center for Computational Science and Engineering of SUSTech.

---

[1] Ashcroft and Mermin, *Solid state physics* (Thomson Learning, 1976).

[2] G. Bergmann, Weak localization in thin films: a time-of-flight experiment with conduction electrons, *Phys. Rep.* **107**, 1 (1984).

[3] P. A. Lee and T. V. Ramakrishnan, Disordered electronic systems, *Rev. Mod. Phys.* **57**, 287 (1985).

[4] H. Suuura and T. Ando, Crossover from Symplectic to Orthogonal Class in a Two-Dimensional Honeycomb Lattice, *Phys. Rev. Lett.* **89**, 266603 (2002).

[5] H.-Z. Lu, J. Shi, and S.-Q. Shen, Competition between Weak Localization and Antilocalization in Topological Surface States, *Phys. Rev. Lett.* **107**, 076801 (2011).

[6] H.-Z. Lu, W. Yao, D. Xiao, and S.-Q. Shen, Intervalley Scattering and Localization Behaviors of Spin-Valley Coupled Dirac Fermions, *Phys. Rev. Lett.* **110**, 016806 (2013).

[7] H.-Z. Lu and S.-Q. Shen, Finite-Temperature Conductivity and Magnetoconductivity of Topological Insulators, *Phys. Rev. Lett.* **112**, 146601 (2014).

[8] B. Fu, H.-W. Wang, and S.-Q. Shen, Quantum Interference Theory of Magnetoresistance in Dirac Materials, *Phys. Rev. Lett.* **122**, 246601 (2019).

[9] H.-W. Wang, B. Fu, and S.-Q. Shen, Anomalous Temperature Dependence of Quantum Correction to the Conductivity of Magnetic Topological Insulators, *Phys. Rev. Lett.* **124**, 206603 (2020).

[10] D. T. Son and B. Z. Spivak, Chiral anomaly and classical negative magnetoresistance of Weyl metals, *Phys. Rev. B* **88**, 104412 (2013).

[11] A. A. Burkov, Chiral Anomaly and Diffusive Magnetotransport in Weyl Metals, *Phys. Rev. Lett.* **113**, 247203 (2014).

[12] X. Huang, L. Zhao, Y. Long, P. Wang, D. Chen, Z. Yang, H. Liang, M. Xue, H. Weng, Z. Fang, X. Dai, and G. Chen, Observation of the Chiral-Anomaly-Induced Negative Magnetoresistance in 3D Weyl Semimetal TaAs, *Phys. Rev. X* **5**, 031023 (2015).

[13] J. Xiong, S. K. Kushwaha, T. Liang, J. W. Krizan, M. Hirschberger, W. Wang, R. J. Cava, and N. P. Ong, Evidence for the chiral anomaly in the Dirac semimetal Na<sub>3</sub>Bi, *Science* **350**, 413 (2015).

[14] J. Wang, H. Li, C. Chang, K. He, J. S. Lee, H. Lu, Y. Sun, X. Ma, N. Samarth, S. Shen, *et al.*, Anomalous anisotropic magnetoresistance in topological insulator films, *Nano Res.* **5**, 739 (2012).

[15] S. Wiedmann, A. Jost, B. Fauqué, J. van Dijk, M. J. Meijer, T. Khouri, S. Pezzini, S. Grauer, S. Schreyeck, C. Brüne, H. Buhmann, L. W. Molenkamp, and N. E. Hussey, Anisotropic and strong negative magnetoresistance in the three-dimensional topological insulator Bi<sub>2</sub>Se<sub>3</sub>, *Phys. Rev. B* **94**, 081302 (2016).

[16] O. Breunig, Z. Wang, A. Taskin, J. Lux, A. Rosch, and Y. Ando, Gigantic negative magnetoresistance in the bulk of a disordered topological insulator, *Nat. Commun.* **8**, 15545 (2017).

[17] X. Dai, Z. Z. Du, and H.-Z. Lu, Negative Magnetoresistance without Chiral Anomaly in Topological Insulators, *Phys. Rev. Lett.* **119**, 166601 (2017).

[18] N. Ma, X.-B. Qiang, Z. Xie, Y. Zhang, S. Yan, S. Cao, P. Wang, L. Zhang, G. Gu, Q. Li, *et al.*, Perpendicular in-plane negative magnetoresistance in ZrTe<sub>5</sub>, *Sci. Bull.* **68**, 1488 (2023).

[19] K. v. Klitzing, G. Dorda, and M. Pepper, New Method for High-Accuracy Determination of the Fine-Structure Constant Based on Quantized Hall Resistance, *Phys. Rev. Lett.* **45**, 494 (1980).

[20] K. S. Novoselov, A. K. Geim, S. V. Morozov, D. Jiang, M. I. Katsnelson, I. V. Grigorieva, S. V. Dubonos, and A. A. Firsov, Two-dimensional gas of massless Dirac fermions in graphene, *Nature* **438**, 197 (2005).

[21] C. Zhang, Y. Zhang, X. Yuan, S. Lu, J. Zhang, A. Narayan, Y. Liu, H. Zhang, Z. Ni, R. Liu, *et al.*, Quantum Hall effect based on Weyl orbits in Cd<sub>3</sub>As<sub>2</sub>, *Nature* **565**, 331 (2019).

[22] F. Tang, Y. Ren, P. Wang, R. Zhong, J. Schneeloch, S. A. Yang, K. Yang, P. A. Lee, G. Gu, Z. Qiao, *et al.*, Three-dimensional quantum Hall effect and metal-insulator transition in ZrTe<sub>5</sub>, *Nature* **569**, 537 (2019).

[23] A. A. Abrikosov, Quantum magnetoresistance, *Phys. Rev. B* **58**, 2788 (1998).

[24] J. Hu and T. Rosenbaum, Classical and quantum routes to linear magnetoresistance, *Nat. Mater.* **7**, 697 (2008).

[25] L. P. He, X. C. Hong, J. K. Dong, J. Pan, Z. Zhang, J. Zhang, and S. Y. Li, Quantum Transport Evidence for the Three-Dimensional Dirac Semimetal Phase in Cd<sub>3</sub>As<sub>2</sub>, *Phys. Rev. Lett.* **113**, 246402 (2014).

[26] A. Narayanan, M. D. Watson, S. F. Blake, N. Bruyant, L. Drigo, Y. L. Chen, D. Prabhakaran, B. Yan, C. Felser, T. Kong, P. C. Canfield, and A. I. Coldea, Linear Magnetoresistance Caused by Mobility Fluctuations in *n*-Doped Cd<sub>3</sub>As<sub>2</sub>, *Phys. Rev. Lett.* **114**, 117201 (2015).

[27] T. Liang, Q. Gibson, M. N. Ali, M. Liu, R. Cava, and N. Ong, Ultrahigh mobility and giant magnetoresistance in the Dirac semimetal Cd<sub>3</sub>As<sub>2</sub>, *Nat. Mater.* **14**, 280 (2015).

[28] C. Shekhar, A. K. Nayak, Y. Sun, M. Schmidt, M. Nicklas, I. Leermakers, U. Zeitler, Y. Skourski, J. Wosnitza, Z. Liu, *et al.*, Extremely large magnetoresistance and ultrahigh mobility in the topological Weyl semimetal candidate NbP, *Nat. Phys.* **11**, 645 (2015).

[29] N. Xin, J. Lourembam, P. Kumaravadivel, A. Kazantsev, Z. Wu, C. Mullan, J. Barrier, A. A. Geim, I. Grigorieva, A. Mishchenko, *et al.*, Giant magnetoresistance

of Dirac plasma in high-mobility graphene, *Nature* **616**, 270 (2023).

[30] S. Li, H.-Z. Lu, and X. C. Xie, Impurity and dispersion effects on the linear magnetoresistance in the quantum limit, *Phys. Rev. B* **107**, 235202 (2023).

[31] K. Ziegler, Scaling behavior and universality near the quantum Hall transition, *Phys. Rev. B* **55**, 10661 (1997).

[32] J. Cserti, Minimal longitudinal dc conductivity of perfect bilayer graphene, *Phys. Rev. B* **75**, 033405 (2007).

[33] K. Ziegler, Minimal conductivity of graphene: Nonuniversal values from the Kubo formula, *Phys. Rev. B* **75**, 233407 (2007).

[34] P. Bhalla, K. Das, D. Culcer, and A. Agarwal, Resonant Second-Harmonic Generation as a Probe of Quantum Geometry, *Phys. Rev. Lett.* **129**, 227401 (2022).

[35] G. D. Mahan, *Many-Particle physics* (Springer Science & Business Media, 2000).

[36] Shon, Nguyen Hong and Ando, Tsuneya, Quantum transport in two-dimensional graphite system, *J. Phys. Soc. Jpn.* **67**, 2421 (1998).

[37] Y. Zheng and T. Ando, Hall conductivity of a two-dimensional graphite system, *Phys. Rev. B* **65**, 245420 (2002).

[38] P. M. Ostrovsky, I. V. Gornyi, and A. D. Mirlin, Electron transport in disordered graphene, *Phys. Rev. B* **74**, 235443 (2006).

[39] S.-Q. Shen, *Topological Insulators: Dirac Equation in Condensed Matter*, Vol. 187 (Springer, 2017).

[40] M. Z. Hasan and C. L. Kane, Colloquium: Topological insulators, *Rev. Mod. Phys.* **82**, 3045 (2010).

[41] X.-L. Qi and S.-C. Zhang, Topological insulators and superconductors, *Rev. Mod. Phys.* **83**, 1057 (2011).

[42] A. H. Castro Neto, F. Guinea, N. M. R. Peres, K. S. Novoselov, and A. K. Geim, The electronic properties of graphene, *Rev. Mod. Phys.* **81**, 109 (2009).

[43] S. Das Sarma, S. Adam, E. H. Hwang, and E. Rossi, Electronic transport in two-dimensional graphene, *Rev. Mod. Phys.* **83**, 407 (2011).

[44] X.-B. Qiang, Z. Z. Du, H.-Z. Lu, and X. C. Xie, Topological and disorder corrections to the transverse Wiedemann-Franz law and Mott relation in kagome magnets and Dirac materials, *Phys. Rev. B* **107**, L161302 (2023).

[45] F. Qin, R. Shen, and C. H. Lee, Nonlinear Hall effects with an exceptional ring, *Phys. Rev. B* **111**, 245413 (2025).

[46] X.-X. Yi, R. Chen, and B. Zhou, Magnetic disorder induced Hall conductance fluctuation in the semi-magnetic topological insulator thin film, *Journal of Physics: Condensed Matter* **37**, 175004 (2025).

[47] F. Qin and R. Chen, Tunable corner states in topological insulators with long-range hopping and diverse shapes, *Phys. Rev. B* **112**, 125405 (2025).

[48] H.-Z. Lu, S.-B. Zhang, and S.-Q. Shen, High-field magnetoconductivity of topological semimetals with short-range potential, *Phys. Rev. B* **92**, 045203 (2015).

[49] H.-W. Wang, B. Fu, and S.-Q. Shen, Intrinsic magnetoresistance in three-dimensional Dirac materials with low carrier density, *Phys. Rev. B* **98**, 081202 (2018).

[50] See Supplemental Material at xx.xxxxxx for theoretical details, which includes Refs. [23, 30, 35, 42, 43, 48, 49].

[51] L. Landau, Diamagnetismus der Metalle, *Z. Phys.* **64**, 629 (1930).

[52] J. S. Dugdale and Z. S. Basinski, Mathiessen's Rule and Anisotropic Relaxation Times, *Phys. Rev.* **157**, 552 (1967).

[53] E. Akkermans and G. Montambaux, *Mesoscopic physics of electrons and photons* (Cambridge university press, 2007).

[54] J. Fang, W. G. Vandenberghe, and M. V. Fischetti, Microscopic dielectric permittivities of graphene nanoribbons and graphene, *Phys. Rev. B* **94**, 045318 (2016).

[55] F. Qin, S. Li, Z. Z. Du, C. M. Wang, W. Zhang, D. Yu, H.-Z. Lu, and X. C. Xie, Theory for the Charge-Density-Wave Mechanism of 3D Quantum Hall Effect, *Phys. Rev. Lett.* **125**, 206601 (2020).